JCI The Journal of Clinical Investigation

HIF-2α activation potentiates oxidative cell death in colorectal cancers by increasing cellular iron

Rashi Singhal, … , Costas A. Lyssiotis, Yatrik M. Shah

J Clin Invest. 2021. https://doi.org/10.1172/JCI143691.

Research In-Press Preview Metabolism Oncology

Graphical abstract

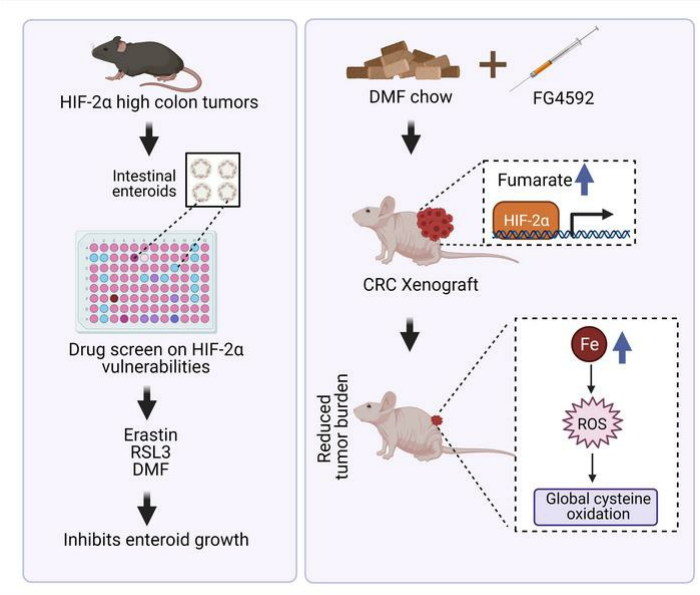

HIF-2α activation potentiates oxidative cell death in colorectal cancers by increasing cellular iron

Rashi Singhal[1], Sreedhar R Mitta[1], Nupur K. Das[1], Samuel A. Kerk[2,3], Peter Sajjakulnukit[3], Sumeet Solanki[1], Anthony Andren[3], Roshan Kumar[4], Kenneth P. Olive [5,6,7], Ruma Banerjee[4], Costas A. Lyssiotis,[1,2,3], Yatrik M. Shah[1,2,3*]

[1]Department of Molecular and Integrative Physiology, [2]Department of Internal Medicine, Division of Gastroenterology, [3]Rogel Cancer Center, [4]Department of Biological Chemistry, University of Michigan Medical School, Ann Arbor, MI 48109. [5]Department of Pathology, [6]Division of Digestive and Liver Diseases, Department of Medicine, [7]Herbert Irving Comprehensive Cancer Center, Columbia University Medical Center, New York, NY 10032

Running title: HIF-2α mediates oxidative cell death in CRC

Correspondence: Yatrik M. Shah, Department of Molecular & Integrative Physiology, Department of Internal medicine, Division of Gastroenterology, University of Michigan Medical School, Ann Arbor, MI 48109. Email: shahy@umich.edu

Disclosure Statement: The authors are not aware of any affiliations, memberships, funding, or financial holdings that might be perceived as affecting the objectivity of this manuscript.

Conflict of Interests: R.B. is a paid member of the scientific advisory board of Apneo Therapeutics and owns equity in the company. C.A.L. is an inventor on patents pertaining to Kras regulated metabolic pathways, redox control pathways in pancreatic cancer, and targeting GOT1 as a therapeutic approach.

Abstract

Hypoxia is a hallmark of solid tumors that promotes cell growth, survival, metastasis and confers resistance to chemo and radiotherapies. Hypoxic responses are largely mediated by the transcription factor hypoxia-inducible factor (HIF)-1α and HIF-2α. Our work demonstrates that HIF-2α is essential for colorectal cancer (CRC) progression. However, targeting hypoxic cells is difficult and tumors rapidly acquire resistance to inhibitors of HIF-2α. To overcome this limitation, we performed a small molecule screen to identify HIF-2α dependent vulnerabilities. Several known ferroptosis activators and dimethyl fumarate (DMF), a cell permeable mitochondrial metabolite derivative, led to selective synthetic lethality in HIF-2α expressing tumor enteroids. Our work demonstrated that HIF-2α integrated two independent forms of cell death via regulation of cellular iron and oxidation. First, activation of HIF-2α upregulated lipid and iron regulatory genes in colon cancer cells and colon tumors in mice and led to a ferroptosis-susceptible cell state. Secondly, via an iron-dependent, lipid peroxidation-independent pathway, HIF-2α activation potentiated ROS, via irreversible cysteine oxidation and enhanced cell death. Inhibition or knock-down of HIF-2α decreased ROS and resistance to oxidative cell death *in vitro* and *in vivo*. Our results demonstrated a mechanistic vulnerability in cancer cells that were dependent on HIF-2α that can be leveraged for colon cancer treatment.

Introduction

Colorectal cancer (CRC) is the third most common cancer and one of the leading causes of cancer-related deaths globally (1, 2). Cancer cells expand rapidly and all solid tumors experience hypoxia due to inadequate vascularization (3). Hypoxia plays a critical role in cancer progression via increasing angiogenesis, glycolysis, apoptotic resistance, therapy resistance, genomic instability and tumour invasion/metastasis (4-6). Hypoxic responses are transcriptionally controlled by hypoxia-inducible factor-1α (HIF-1α), HIF-2α, and HIF-3α, which are members of the basic helix–loop–helix-PER-ARNT-SIM (bHLH–PAS) family (7). HIFs regulate multiple pathways involved in cell proliferation, survival, apoptosis, migration, metabolism, and inflammation (8, 9). HIF-1α and HIF-2α exhibit distinct roles in colon cancers (10-12).

HIF-1α is positively associated with the malignant progression of various tumor entities (13). However, the role of HIF-1α in CRC is controversial and disruption or constitutive activation of HIF-1α in intestinal epithelial cells did not alter colon adenoma formation (14). In contrast, HIF-2α is essential for CRC growth and progression in cell culture and *in vivo* (15-18). Activation of intestinal epithelial HIF-2α induces a potent epithelial proinflammatory response by regulating the expression of inflammatory cytokines and chemokines (19). Our recent work has demonstrated an essential role for epithelial HIF-2α-elicited inflammation and regulation of intra-tumoral iron homeostasis in colon cancer (16). Recently, PT2385, a selective, potent and orally active small-molecule was shown to selectively inhibit HIF-2α by blocking dimerization with its partner protein, aryl hydrocarbon receptor nuclear translocator (ARNT) (20). PT2385 efficiently inhibits the expression of target genes in clear cell renal cell carcinoma (ccRCC) cells and tumor xenografts (21, 22) and is in Phase 2 clinical trial in patients with advanced ccRCC. However, other strategies are needed to target HIF-2α expressing cancer cells as resistance to

PT2385 arises rapidly (21, 22). Moreover, there is an urgent need to increase clinical benefits of known anticancer therapies by recognizing tumor cell-specific vulnerabilities. Herein, we performed an unbiased screen in tumor enteroids with HIF-2α overexpression with the aim of identifying hypoxic tumor-cell specific vulnerabilities. Interestingly, HIF-2α expression potently sensitized tumor enteroids to ferroptotic activators such as erastin, RSL3 and sorafenib and to dimethyl fumarate (DMF). Ferroptosis is a nonapoptotic, iron-dependent form of oxidative cell death (23) characterized by the loss of lipid peroxide repair by the glutathione peroxidase GPX4, an increase in free iron, and the oxidation of polyunsaturated fatty acid (PUFA)-containing phospholipids (24). Activating ferroptosis has emerged as a potent mechanism for targeting cancer cells *in vivo* (25-27).

DMF is a cell permeable dimethyl ester of fumaric acid and an FDA approved drug for the treatment of relapsing forms of multiple sclerosis and psoriasis due to its immunomodulatory properties (28, 29). Numerous studies have shown that DMF has antioxidant and cytoprotective effects in non-malignant models (28, 30, 31) via its activation of the nuclear factor erythroid 2 (NF-E2)-related factor 2 (NRF2) pathway (28, 30-33). In parallel, several *in vitro* studies have suggested that DMF is cytotoxic to a variety of cancer cell lines (34-37). However, the underlying mechanisms have remained obscure.

In the present study, we report that HIF-2α activation is essential in the cellular vulnerability to oxidative cell death. Hypoxia or hypoxic mimetics via HIF-2α stabilization synergize with pro-oxidants to potentiate an increase in ROS and lipid ROS and a decrease in glutathione production, inducing cell death. Mechanistically, we reveal that activation of HIF-2α increases cellular iron to enhance ferroptosis and/or irreversible cysteine oxidation leading to cell death, which can be protected by hydrogen sulfide or its precursor, 3-mercaptopyruvate. These findings

highlight HIF-2α-dependent tumor lethality via iron-dependent lipid and protein oxidation that has implications for the development of novel therapeutics for the improved treatment of colon cancer.

RESULTS

Drug screen identifies synthetic vulnerability to HIF-2α in tumor enteroids.

Adenomatous polyposis coli (APC) is a tumor suppressor protein mutated in more than 80% of patients with sporadic colon cancer (38). The Cdx2-ER^{T2}Cre; *Apc$^{fl/fl}$* mouse model enables tamoxifen inducible deletion of both *Apc* alleles in intestinal epithelial tissues. These mice were crossed with *HIF2α$^{LSL/LSL}$* mice, which harbor oxygen-stable HIF-2α alleles flanked by loxP-Stop-loxP cassette (Figure 1A) (39). In Cdx2-ER^{T2}Cre; *Apc$^{fl/fl}$HIF2α$^{LSL/LSL}$* mice, tamoxifen treatment results in a robust induction of HIF-2α and disrupts *Apc* specifically in colon epithelial cells. Enteroids were isolated from these two mouse models, cultured with a panel of chemotherapeutics and growth was monitored for 5 days (Figure 1A). Colon tumor enteroids overexpressing HIF-2α were resistant to carboplatin, cisplatin, cyclophosphamide and oxaliplatin compared to enteroids from Cdx2-ER^{T2}Cre; *Apc$^{fl/fl}$* (Supplemental Figure 1). This data is consistent with the well-known role of HIF signaling in chemo-resistance (5). Tumor enteroids from Cdx2-ER^{T2}Cre; *Apc$^{fl/fl}$* mouse were highly sensitive to drugs such as doxorubicin, mitoxantrone, irinotecan and eribulin unlike tumor enteroids from Cdx2-ER^{T2}Cre; *Apc$^{fl/fl}$HIF2α$^{LSL/LSL}$* (Figure 1B). RSL3, sorafenib, erastin and DMF ranked as the most effective small molecules that significantly reduced the growth of tumor enteroids from Cdx2-ER^{T2}Cre; *Apc$^{fl/fl}$HIF2α$^{LSL/LSL}$* in comparison to CDX2-CreER^{T2}*Apc$^{fl/fl}$* (Figure 1C). Erastin and RSL3 are classic ferroptosis activators (23), which inhibit xCT, encoded by the *Slc7a11* gene and is component of system x_C^- and glutathione peroxidase 4 (GPX4), respectively. DMF is not a known regulator of ferroptosis and is a cell permeable mitochondrial derivative that is cytotoxic in several cancer cell lines (Figure 1D). Together, these results suggest that HIF-2α expressing tumors can be selectively targeted by oxidative stress activators.

HIF activation synergizes with ferroptotic activators in colon cancer cells.

Erastin and RSL3 are classical inducers of ferroptosis that were originally identified in a screen for small molecules that are selectively lethal to cancer cells (23). Recently, ccRCC-derived cell lines were reported to require HIF-2α activation to exhibit vulnerability to ferroptosis (40). We demonstrate that the hypoxic mimetic FG4592 or hypoxia significantly potentiated cell death following treatment of ferroptosis inducers erastin (Supplemental Figure 2) and RSL3 (Supplemental Figure 3) in a HIF-2α dependent manner (Supplemental Figure 4A-C). It is important to note that FG4592 treatment alone had no effect on growth in cell lines (Supplemental Figure 4D) whereas hypoxia decreases growth in CRC cells (Supplemental Figure 4E). Expression of two lipid genes important in ferroptosis sensitization in renal cancers, hypoxia inducible lipid droplet associated protein (HILPDA) and perilipin 2 (PLIN2) and aberrant generation of lipid ROS were increased following FG4592 treatment (Supplemental Figure 5, A and B) and this increase was HIF-2α dependent (Supplemental Figure 5C), implicating the role for HIF-2α in driving ferroptosis through the accumulation of oxidized lipids. To examine the role of HIF-2α in regulating ferroptosis *in vivo*, Villin-CreER^{T2}-*HIF2α*$^{LSL/LSL}$ were crossed with *Slc7a11*$^{fl/fl}$ mice. Tamoxifen treatment enables the intestine-specific deletion of *Slc7a11*(Supplemental Figure 6A) and overexpression of HIF-2α (Supplemental Figure 6B). The colonic tissue from these mice were analyzed for histological changes 14 days following last tamoxifen dose (Figure 2A). The deletion of *Slc7a11* or overexpression of HIF-2α alone where indistinguishable from control littermates (Figure 2B). However, disruption of *Slc7a11* in combination with HIF-2α overexpression led to colonic epithelial degeneration and vacuolization (Figure 2B). Lipid peroxide induced oxidative stress was measured by 4-hydroxy 2-nonenal (4-HNE) staining (Figure 2C). The Villin-

CreER^{T2}*Slc7a11*$^{fl/fl}$; *HIF2α*$^{LSL/LSL}$ mice showed a robust increase in histological score (Figure 2D) and 4-HNE intensity (Figure 2E), clearly indicating increased oxidative stress and epithelial cell loss in these mice in comparison to their littermate controls. Furthermore, HILPDA and PLIN2 mRNA levels were significantly increased in Villin-CreER^{T2}-*HIF2α*$^{LSL/LSL}$ mice compared to littermate controls (Figure 2F). Since iron accumulation is involved in lipid induced oxidative stress and cell death, we also measured iron levels in liver and intestinal tissue of these mice. We observed higher levels of both liver and intestinal iron in Villin-CreER^{T2}-*HIF2α*$^{LSL/LSL}$ mice compared to littermate controls (Figure 2G). The liver iron increase is due to increase iron absorption from the small intestine. This data confirms the role of HIF-2α in ferroptosis sensitization in vivo and suggest that drugs that induce ferroptosis could be highly efficacious in killing hypoxic cells.

HIF activation promotes DMF-induced cell death in CRC cells.

Current ferroptosis inducers have poor *in vivo* bioavailability in contrast to DMF, an FDA approved oral drug for the treatment of multiple sclerosis that has fewer side effects than several other drugs (28, 29, 41). Our screen identified DMF as a small molecule effective in reducing the growth of hypoxic tumor enteroids (Figure 1C). A panel of colon cancer cell lines were treated with DMF either alone or in combination with hypoxia or hypoxia mimetic, FG4592. Our data showed a dose dependent inhibition of colon cancer cell growth by DMF (Supplemental Figure 7A). FG4592 potentiated DMF-induced CRC cell death as assessed by MTT and long-term clonogenic survival assays (Figure 3 A, B and C). Additionally, the cells treated with DMF and cultured in hypoxia were less viable (Figure 3, D and E) and showed decrease cell growth (Supplemental Figure 7B) in comparison to normoxia. HIF-2α levels were monitored following treatment and showed increase in FG4592 or DMF and FG4592 (Supplemental Figure 7C). The

effect of DMF and FG4592 or hypoxia combination is highly potent to inhibit CRC cell growth as confirmed by IC50 (Figure 3F). Consistent with the erastin and RSL3 data, HIF-2α was essential for promoting DMF mediated inhibition of CRC cell growth (Figure 3G).

DMF induces cell death independent of ferroptosis.

Since DMF was effective in decreasing hypoxic cell growth along with other ferroptotic activators (Figure 1C), we assessed whether DMF mediates ferroptotic cell death. For this, HCT116 and SW480 cells were treated with DMF with or without the ferroptosis inhibitors ferrostatin-1 (Fer-1) or liproxstatin-1 (Lip-1) (23, 29). Fer-1 and Lip-1 did not rescue cell death and viability following DMF treatment, whereas RSL3-mediated cell death was rescued by Fer-1 and Lip-1 (Figure 4A and Supplemental Figure 8A). Moreover, DMF only marginally increased lipid ROS in HCT116 cells and Fer-1 did not prevent this induction, whereas in SW480, DMF did not increase lipid ROS (Figure 4B). In contrast, lipid ROS induction by RSL3 was significantly attenuated by Fer-1 (Figure 4B). DMF can react directly with the antioxidant glutathione (GSH), leading to decreased NADPH levels and enhanced ROS (42). Consistent with these data, DMF significantly decreased cellular GSH levels comparable to erastin and RSL3 (Supplemental Figure 8B). To assess if the HIF-dependent potentiation of cell death is due to synergizing with compounds that reduce GSH pools, we used buthionine sulfoximine (BSO), which inhibits de novo GSH biosynthesis. DMF either alone or in combination with BSO decreased GSH levels in HCT116 and SW480 cells (Supplemental Figure 8, B and C). Treatment with FG4592 alone or in combination with BSO also decreased cellular GSH levels (Supplemental Figure 8, B and C). However, cell viability was not decreased with the co-treatment of BSO and FG4592 (Supplemental Figure 8D), suggesting GSH depletion is not the major mechanism of cell death after DMF and FG4592 co-treatment.

Fumarate is a TCA cycle metabolite and a potent electrophile (43). DMF inhibits GAPDH via covalent modification of a reactive cysteine, and consequently aerobic glycolysis (44) (Figure 4C). We explored the impact of DMF on the metabolome using an LC-MS/MS-based profiling approach (45, 46). The metabolomics data shows an abundance of glycolytic intermediates upstream and downstream of GAPDH in HCT116 and SW480 cells treated with DMF (Figure 4D; full metabolomics data in Supplemental Table 1). Further, and consistent with the well characterized role of HIF-2α in glycolysis, several glycolytic intermediates were increased with FG4592 treatment. However, cell viability was not decreased with the co-treatment of FG4592 and glycolytic inhibitors (Figure 4E). These results indicate that alternative mechanisms are involved in DMF-mediated cell death of hypoxic cancer cells.

ROS accumulation and iron-toxicity are essential in DMF-induced HIF-2α-mediated cell death

Our work thus far ruled out ferroptosis, GSH depletion, and inhibition of glycolysis as being relevant to DMF-sensitized cell death. Since DMF is an electrophile, we examined the effect of other electrophiles, dimethyl itaconate (DMI) and 4-octyl itaconate (4-OI) (47), on cell growth. Both DMI and 4-OI decreased cellular growth, which was potentiated by co-treatment with FG4592 (Supplemental Figure 9, A and B).

Supplementation of growth media with the cysteine precursor, N-acetyl cysteine (NAC), rescued HCT116 and SW480 cell death and viability treated with DMF with or without FG4592 (Figure 5A and Supplemental Figure 9C). Similar results were observed with DMF treatment and cells maintained in hypoxia (Figure 5B). Interestingly, FG4592 or hypoxia treatment alone increased ROS as assessed by the cell-permeant 2',7'-dichlorodihydrofluorescein diacetate (H_2DCFDA), which is used as an indicator for reactive oxygen species (ROS) (Figure 5, C and D). Co-

treatment with DMF potentiated this increase in ROS generation which was rescued with NAC (Figure 5, C and D). To confirm that the sensitivity towards oxidative cell death is mediated via HIF-2α, shRNA mediated HIF-1α and HIF-2α knock-down cells were utilized. The ROS levels were drastically reduced in HIF-2α knock-down cells (Figure 5E), suggesting the role of HIF-2α in ROS production after DMF treatment. To further confirm the role of HIF-2α, we employed a HIF-2α-specific inhibitor PT2385 (21, 22), which decreased ROS in FG4592 and DMF treated CRC cells (Supplemental Figure 9D).

Since HIF activation can lead to changes in mitochondrial metabolism (48) and ROS production, we analyzed whether DMF or FG4592 treatment induced changes in mitochondrial metabolites pools. However, significant changes in the levels of mitochondrial metabolites were not seen suggesting that HIF-2α influences cellular ROS via other mechanisms (Figure 5F; full metabolomics data in Supplemental Table 1). RNA-seq data from a HIF-2α overexpression mouse model (49) analyzed for oxidant generating enzymes revealed upregulation of lysyl oxidase (LOX) and cyclooxygenase (COX) (encoded by *Ptgs* gene) (Supplemental Figure 10A). However, the viability of HCT116 and SW480 cells treated with DMF and FG4592 was only slightly improved using LOX and COX inhibitors (Supplemental Figure 10B).

We have previously demonstrated that HIF-2α is critical for cellular iron uptake, which leads to ROS generation via the Fenton reaction (50). Consistent with our previous work, FG4592 and hypoxia increased cellular iron in CRC cells (Supplemental Figure 10, C and D). The increase in iron levels after hypoxia or FG4592 treatment was dependent on HIF-2α (Supplemental Figure 10D). Interestingly, the cell-death mediated by DMF and FG4592 was rescued in low-iron versus control media (Figure 5G). Moreover, ROS production induced by DMF, FG4592 or DMF and

FG4592 co-treatment was attenuated in low-iron medium compared to control (Figure 5H). Together, these data suggest a novel mechanism linking iron toxicity via HIF-2α and vulnerability to oxidative stress.

Protective persulfidation via H_2S can rescue DMF and HIF-2α-induced cell death

Since metal catalyst oxidation is a central mechanism for DNA damage (51), we checked the expression of γH2AX, a sensitive marker of DNA damage and repair (52). Western blot analysis revealed a robust increase in the expression of γH2AX in HCT116 and SW480 cells treated with DMF, however, the increase was not significant when cells were co-treated with DMF and FG4592 (Supplemental Figure 11A). We next assessed if irreversible protein oxidation is involved in DMF and FG4592 induced cell death. Hydrogen sulfide (H_2S) can protect against overoxidation of cysteine thiols via persulfidation, a posttranslational modification (53) (Figure 6A). We therefore assessed whether Na_2S or 3-mercaptopyruvate (3-MP), a substrate for mercaptopyruvate sulfurtransferase (54), by increasing intracellular H_2S, protect cells from DMF and FG4592-induced cell death. Both 3-MP and Na_2S rescued cell viability following co-treatment with DMF and FG4592 (Supplemental Figure 11, B and C). Interestingly, H_2S did not rescue cells from erastin or RSL-3 induced cell death (Supplemental Figure 11, D and E). To rule out that the protective role of H_2S was not due to DMF depletion resulting from the nucleophilic addition of the sulfide anion on DMF, Na_2S and 3-MP were added to fresh medium 16 h after initiation of cell death by DMF and FG4592 or DMF and hypoxia (Figure 6B). Na_2S and 3-MP protected against cell death even under these conditions (Figure 6, C and D and Supplemental Figure 11F). Further, intracellular ROS levels induced by DMF or DMF and FG4592 were decreased upon supplementation with 3-MP and Na_2S (Figure 6E). These data are consistent

with the model that the potentiation of HIF-induced cell death by DMF involves oxidative protein damage, which is protected by H_2S.

FG4592 potentiates DMF-mediated CRC cell death in vivo.

We next assessed the *in vivo* efficacy of DMF and FG4592 co-treatment in established CRC tumors. For this, HCT116, SW480 and DLD1 cells were implanted subcutaneously into the flanks of immunocompromised mice and allowed to establish for 10 days prior to DMF and FG4592 treatment (Figure 7A). CRC cell xenografts exhibited profound growth inhibition upon DMF and FG4592 treatment; both tumor volume (Figure 7B) and tumor weight (Figure 7C) were significantly reduced in all the three xenografts compared to vehicle or treatment with the individual drugs. Tumor cell proliferation as assessed by the BrdU incorporation assay was also decreased in HCT116, SW480 and DLD1 xenografts with DMF and FG4592 co-treatment (Figure 7D). However, tumor fumarate levels were not significantly different between the DMF only and the DMF and FG4592 co-treatment groups in all 3 CRC-xenograft mice (Supplemental Figure 12A). The tumors in response to different treatments do not show any major histological changes (Supplemental Figure 12B). However, the percentage of TUNEL-positive apoptotic cells was increased in all three xenografts co-treated with DMF and FG4592 (Figure 7E). DMF+FG4592 was not cytotoxic to normal tissues in mice as confirmed by histological analysis of colon tissue and normal serum ALT and AST levels (Supplemental Figure 12, C and D). Consistent with the known roles of hypoxia in erythropoiesis (55, 56), erythropoietin, hematocrits, hemoglobin, and red blood cells were increased with FG4592 treatment alone or in combination with DMF (Supplemental Figure 12E). Together, these data demonstrate that hypoxic tumor cells are highly vulnerable to DMF treatment, highlighting a potential therapeutic window.

DMF-mediated CRC cell death in vivo is HIF-2α dependent.

To confirm the role of HIF-2α in DMF-mediated CRC cell death in-vivo, we utilized HIF-2α knock-down HCT116 cells. Stable non-target scrambled and HIF-2α knock-down HCT116 cells were injected subcutaneously into both flanks of immunocompromised mice and allowed to grow for 10 days prior to DMF and FG4592 treatment (Figure 8A). HIF-2α knock-down cells were resistant to DMF and FG4592 treatment. Cells expressing scrambled shRNA showed a significant reduction in tumor volume and weight in mice treated with DMF+FG4592, whereas the HIF-2α knock-down cells where completely resistant (Figure 8, B and C). Similarly, tumor proliferation and apoptosis was not altered in HIF-2α knock-down cells following DMF+FG4592 treatment (Figure 8, D and E). These data demonstrate that HIF-2α activation increases vulnerability to oxidative cell death *in vivo*.

Discussion

Our work demonstrates that HIF-2α via an increase in cellular iron is an important source of ROS, which coupled to posttranslational protein modification by DMF or lipid-ROS induction by ferroptosis-inducing agents, leads to cell death (Figure 8F). HIF-2α is the major transcriptional regulator of cellular iron levels (50). Our work now connects the HIF-2α dependent increase in cellular iron with ROS, which enhances the vulnerability of the proteome to oxidative damage and in the presence of the electrophile DMF, stimulates cell death. A central role of basal HIF-2α is in increasing cellular ROS, which is mimicked by FG4592 in a HIF-2α dependent manner, and we now demonstrate that this is essential in oxidative cell death pathways.

Apart from leading to oxidative stress, ROS can also transduce signals by reversibly modifying the redox state of cysteine residues in proteins. Cysteine thiols in proteins can be oxidized to sulfenic acid (RSOH), sulfinic acid (RSO_2H), and sulfonic acid (RSO_3H), which are associated with pathophysiological processes (57). H_2S mediated persulfidation protects proteins from irreversible oxidation (58) as the cysteine persulfide or its oxidation products (e.g. Cys-S-S-sulfonate), can be reduced to a cysteine thiolate by thioredoxin (59, 60). Fumarate itself can covalently modify cysteines, and numerous protein targets of this posttranslational modification have been identified (43). Although considerable heterogeneity in the proteins targeted by fumarate is seen in different cell lines, proteomic analysis reveals that tumor suppressors and signaling proteins are a highly enriched class of modified proteins. Our data demonstrates that protein oxidation might be a major mechanism of cell death following DMF because DMF and FG4592/hypoxia co-treatment is abrogated by protective persulfidation by H_2S. While a single bolus administration of H_2S was used in the present study, it is important to note that CRCs are

exposed to high H_2S levels derived from microbial metabolism. High concentrations of H_2S inhibit the electron transport chain and repeated long-term exposure is growth restricting (61). The present work suggests that H_2S might confer protection against oxidative stress to tumors and further work is in needed to define its role in CRCs in vivo.

In vivo disruption of *Slc7a11* with a simultaneous increase in HIF-2α led to increased histological intestinal damage and the hallmarks of ferroptosis in normal intestine. Previous work has demonstrated that the susceptibility to ferroptosis following HIF-2α activation is not only iron dependent but also requires lipid reprogramming via HIF-2α (40). However, pharmacological activation of HIF-2α with DMF did not lead to heightened intestinal injury in normal tissue, illustrating a considerable therapeutic window. Moreover, it was elegantly shown by Taniguchi et al, that activation of HIF-2α was protective in radiation-induced damage (62), and HIF-2α dependent iron oxidation and cell death were not observed (62). Elevated ROS is a hallmark of most cancers but need to be precisely balanced by antioxidant genes for tumor progression. There are numerous studies which have highlighted the inhibitory role of HIF-1α towards ROS production. HIF-1α regulates redox homeostasis by regulating the levels NADPH and GSH. HIF-1α is also known to promote mitochondrial selective autophagy and thus lowering the mitochondrial mass which suppresses the oxidation of both glucose and fatty acids and decreases mitochondrial ROS production under hypoxic conditions (63). On the contrary, in our study we have identified strong association of HIF-2α with ROS production. HIF-2α activation tips the balance toward ROS-induced cell death and thus providing specificity to cancer cells compared to normal tissues.

We show that HIF-2α potentiates cell death via ferroptosis activators and DMF, and both pathways require iron. Interestingly, these oxidative pathways have distinct and non-overlapping

mechanism of cell death. HIF-2α potentiation of ferroptosis can be completely rescued with lipid ROS scavengers liproxstatin-1 and ferrostatin-1, but these compounds have no effects on DMF or DMF+ FG4592 mediated cell death. Similarly, reversing protein oxidation via H_2S can rescue DMF mediated cell death, but does not protect against ferroptosis induced by erastin or RSL3. It is unclear how the HIF-2α -induced increase in iron-dependent ROS generation regulates distinct cell death pathways, hence becomes an active area for future studies.

HIF-2α inhibitors that are in clinical trials have shown promise although acquired resistance to them is a major limitation for long-term efficacy (21, 22). Our work suggests caution if the PT2385 inhibitor is used in an adjuvant setting with known chemotherapeutics that rely on ROS generation. While HIF-2α inhibitors can be used to target cancers that rely on HIF-2α for progression, we demonstrate mechanisms by which HIF-2α activation can be therapeutically leveraged as a synthetic lethality. FG4592 is currently in clinical trials for treating anemia in chronic kidney disease (NCT01750190; ClinicalTrials.gov). DMF is clinically used for relapsing multiple sclerosis and psoriasis. Our *in vivo* study on mouse xenograft-colon cancer model shows the potential utility of this drug combination against colorectal cancer. However, it is important to note that DMF by itself does not reduce tumor growth *in vivo,* which could be related to the degree of hypoxia and HIF-2α activation in tumor tissue. Therefore, HIF-2α stabilizers such as FG4592 that induce robust HIF-2α induction are needed to increase the anti-tumoral efficacy of DMF. Erastin and RSL3 have been used as ferroptosis inducers in mostly *in vitro* experiments because of the limited in vivo bioavailability and reduced metabolic stability. However, studies have used imidazole ketone erastin (IKE) which is a derivative of erastin with nanomolar potency, increased solubility, and metabolic stability. IKE has been shown to inhibit tumor growth in a diffuse large B cell lymphoma mouse model (64). In conclusion, our study has

unmasked the role of HIF-2α in driving the synthetic lethality of hypoxic CRC cells to oxidative stress-inducing compounds like DMF and exposed the potential for exploiting this intrinsic vulnerability for chemotherapeutic development.

Methods

Animal Experiments

All animal studies were carried out in accordance with Institute of Laboratory Animal Resources guidelines and approved by the University Committee on the Use and Care of Animals at the University of Michigan (IACUC protocol number: PRO00008292) For all experiments, male and female mice, 6 to 8-weeks of age were used. All mice are a C57BL/6 background maintained in standard cages in a light- and temperature-controlled room and were allowed a standard chow diet and water ad libitum. Villin-CreER^{T2} *HIF2α*$^{LSL/LSL}$ and *Apc*$^{fl/fl}$ mice have been previously described(16, 39) . These mice were crossed with the colon specific Cre to generate the CDX2-CreER^{T2}-*Apc*$^{fl/fl}$; *HIF2α*$^{LSL/LSL}$ mice. Correctly targeted ES cells in which exon 3 of *Slc7a11* was flanked by Lox-P (*Slc7a11*$^{fl/fl}$) sites were generated by the International Mouse Phenotyping Consortium. *Slc7a11*$^{fl/fl}$ mice were also crossed to the Villin-CreER^{T2} mice and further crossed to the *HIF2α*$^{LSL/LSL}$ mice *to generate the* Villin-CreER^{T2}-*Slc7a11*$^{fl/fl}$*;HIF2α*$^{LSL/LSL}$ mice. For all experiment's littermate controls were used and the Cre recombinase was activated by I.P injection with tamoxifen in corn oil (100 mg/kg) for three consecutive days and were euthanized 1 week or 2 week following the last tamoxifen treatments.

Cell lines and reagents

HCT116, SW480, DLD1, RKO, HT29, MC38 and CT26 cells were obtained from ATCC and grown in DMEM with L-glutamine, D-glucose, and sodium pyruvate (GIBCO) supplemented with 10% heat-inactivated FBS and 1% antibiotic-antimycotic mix (Invitrogen). All cells were maintained in a humidified environment at 37 °C and 5% CO_2 in a tissue culture incubator. For hypoxic treatment, cells were maintained in a humidified environment at 37 °C and 1% O_2 and

5% CO_2 tissue culture incubator. DMF, BSO, BAPN and Nimulside were purchased from Sigma-Aldrich (St. Louis, MO, USA). Erastin, RSL3, FG4592, Ferrostatin-1(Fer-1), Liproxstatin-1(Lip-1) and N-acetyl cysteine (NAC) were purchased from Cayman chemical. 3-MP was purchased from Santa Cruz Biotechnology.

C11-BODIPY lipid ROS measurement

$1x10^6$ HCT116 or SW480 cells were seeded in 12-well plates and allowed to adhere overnight at 37 °C. The day before the experiment, cells were treated with DMSO (vehicle), erastin (5 μM), RSL3 (2 μM) or DMF (50 μM), ferrostatin -1(Fer-1) (1 μM) with or without FG4592 (100 μM) and incubated for 12 h at 37 °C. Cells were harvested using PBS-EDTA(5mM), buffer, washed once with HBSS and suspended in HBSS containing 5 μM C11-BODIPY (ThermoFisher) and incubated at 37 °C for 30 min. Cells were pelleted, washed and resuspended in HBSS. Fluorescence intensity was measured on the FITC channel using Beckman Coulter MoFlo Astrios. A minimum of 20,000 cells was analyzed per condition. Data was analyzed using FlowJo software (Tree Star, Ashland, OR, USA). Values are expressed as mean fluorescence intensity (MFI).

ROS detection assay

The cell-permeable free radical sensor carboxy-H2DCFDA (Invitrogen) was used to measure intracellular ROS levels. For HIF-2α knock-down (shHIF-2α) and non-target (sh scrambled) HCT116 and SW480 cells, CellROX™ Deep Red Reagent (TheromoFisher) was used due to the limitation of plasmid (pGipZ) backbone which has internal green fluorescence. Cells treated with DMF (50 μM), FG4592(100 μM) or subjected to hypoxia (1% O_2) with or without N-acetyl cysteine (NAC) (5mM) were harvested by ice-cold PBS-EDTA(5mM) buffer and incubated with

10 μM carboxy-H2DCFDA or 2.5 μM CellROX dye in PBS at 37°C for 30-45 min. The cells were washed, resuspended in PBS, and analyzed using Beckman Coulter MoFlo Astrios flow cytometer. Data were analyzed using FlowJo software. Values are expressed as the percentage of cells positive for DCF fluorescence or Mean fluorescence intensity in case of CellROX dye.

MTT cell viability assay

2000-3000 cells were seeded in a 96-well plate and allowed to adhere overnight at 37 °C. The next day cells were treated with FG4592(100 μM) or for 16 hours in co-treatment conditions. The cells were then treated with different agents as indicated in figures. In Hypoxia experiments, treated cells were cultured in hypoxic incubator for 3 days. 24-hours following treatment a Day 0 reading was taken. Following the Day 0 read, the corresponding treatment and readings were taken every 24-hours for 72-hour assay. Cells were incubated for 45 minutes with Thiazolyl Blue Tetrazolium Bromide (Sigma) then solubilized with dimethyl sulfoxide. Absorbance was taken at 570nm. All reads were taken in technical triplicates.

Clonogenic assay

Cells were plated in a 6-well plate in biological triplicates at 300-600 cells per well in 2mL of media. After 48 hours, cells were treated with different reagents as mentioned in figure legends. In case of Hypoxia experiments, cells were treated with DMF and subjected to hypoxia for 48 hours, after which they were maintained under ambient oxygen environments. Assays were concluded after 10-15 days by fixing in cold 10% buffered formalin for 10 min and staining with 0.5% crystal violet 20% methanol solution for 30 min. Colonies were manually counted via study-blinded observer.

LDH cell-death assay

The cell-death was measured using LDH cytotoxicity assay kit from Takara Bio (CA, USA). 5000-10,000 cells were seeded in a 96-well plate and allowed to adhere overnight at 37 °C. The next day cells were treated with FG4592(100 μM) for 16 hours in co-treatment conditions. The cells were then treated with different agents as indicated in figures. In case of Hypoxia experiments, cells were treated with different reagents and cultured in hypoxic conditions (1% O_2). Supernatants were harvested after 48-hour treatment and a media only control and a triton control were also included. The supernatant was incubated with LDH detection reagent for 30 minutes as per the manufacturer instructions. Absorbance was taken at 490nm. All reads were taken in technical triplicates. The cytoxicity/cell death was calculated using the formula mentioned as per the manufacturer protocol.

Metabolomics

Cells were plated at 500,000-1 million cells per well in 6-well plates. After 24 hours, cells were treated with DMF (50μM) and FG4592 (100μM) for another 24 hours. After treatment, cells were washed once with ice cold 1X PBS followed by an incubation with ice cold 80% methanol on dry ice for 10 minutes. Cells were then scraped, and the polar metabolite supernatant was collected in a 1.5 mL tube on dry ice. Samples were clarified via centrifugation at max speed for 10 minutes at 4°C. The supernatant was then transferred to a fresh tube at stored at -80°C until analysis. Protein concentration was determined by processing a parallel well/dish for each sample and used to normalize metabolite fractions across samples. Based on protein concentrations, the cell solutions were transferred to a fresh micro centrifuge tube and lyophilized using a SpeedVac concentrator. Dried metabolite pellets were re-suspended in 45 μL 50:50 methanol:water mixture for LC–MS analysis. Data was collected using previously

published parameter (45, 65). The QqQ data were pre-processed with Agilent MassHunter Workstation Quantitative Analysis Software (B0700). Additional analyses were post-processed for further quality control in the programming language R. Finally, each metabolite abundance level in each sample was divided by the median of all abundance levels across all samples for proper comparisons, statistical analyses, and visualizations among metabolites. The statistical significance test was done by a two-tailed t-test with a significance threshold level of 0.05

GSH assay

HCT116 and SW480 cells plated in a 96-well plate were treated with different agents or the vehicle for 24 hours. The GSH concentrations were determined using the GSH-Glo Glutathione Assay Kit (Promega) as per the manufacturer's instructions. The luminescence-based assay is based on the conversion of a luciferin derivative into luciferin in the presence of GSH, catalyzed by glutathione *S*-transferase. Luciferase expression was then measured on a Synergy Mx Microplate Reader (BioTek). The signal generated in a coupled reaction with firefly luciferase is proportional to the amount of GSH present in the sample. The concentration was determined through a standard curve using GSH standard solution provided with the kit.

Western blotting

HCT116 and SW480 cells were seeded at 1m/mL density in a 6 well plate in triplicates for each condition and allowed to adhere overnight. Cells were lysed with radioimmunoprecipitation (RIPA) assay buffer with added protease (1:100 dilution; Sigma) and phosphatase (1:100 dilution; ThermoFisher Scientific) inhibitors. After cell lysis, solubilized proteins were resolved on 10% SDS-polyacrylamide gels and transferred to nitrocellulose membrane, blocked with 5% milk in TBST and were immunoblotted with the indicated primary antibodies made at 1:1000

dilution in blocking solution for HIF-1α(Abcam), HIF-2α (Bethyl lab), γH2AX(Abcam) and β-actin (Proteintech).

Histology and 4-HNE staining

Colonic tissues or tumor tissues were rolled and fixed with PBS-buffered formalin for 24-hours followed by embedding in paraffin. 5μM sections were stained for Hematoxylin-and-eosin (H & E) and mounted with permount mounting medium (Fisher scientific). For, 4 hydroxy-2-noneal/4-HNE staining, paraffin-embedded tissue sections were subjected to antigen retrieval, followed by blocking with 5% goat serum in PBS and probed with primary antibody against 4-HNE (1:200 dilutions, BS6313R, Bioss). Sections were then washed three times with PBST and were incubated with HRP conjugated anti-rabbit IgG (1:500 Dilution, Cell Signaling technology) for 1 h. Sections were then washed three times with PBST and incubated with DAB substrate solution to sufficiently cover them. After the sample color turned brown, the reaction was stopped by distilled water and dehydration steps were carried. The slides were mounted using permount mounting medium.

Tumor enteroid screening

Mouse colonic crypts were isolated using a previously described method(66). Colon was isolated from CDX2-ER^{T2}Cre; *Apc*$^{fl/fl}$ *HIF2α*$^{LSL/LSL}$ and CDX2-ER^{T2}Cre; *Apc*$^{fl/fl}$ mice and cut in to 1cm pieces. Tissue was incubated in 10mM DTT for 15 minutes at room temperature. Tissues were rinsed with DPBS supplemented with gentamicin and primocin. Tissue was incubated with slow rotation at 4C for 75 minutes in 8mM EDTA. EDTA was removed and tissue was put through three cycles of snap-shakes to release crypts. Isolated crypts were spun down and collected in cold LWRN medium. Crypts were then plated in matrigel (Corning) in 96-well culture plates in

LWRN media and imaged using Image express Micro. Enteroids were treated with indicated drugs/inhibitors (10μM) and growth was monitored after 5 days.

RNA isolation and RNA-seq and qPCR analysis

HCT116 and SW480 cells were seeded at 1m/mL density in a 6 well plate in triplicates for each condition and allowed to adhere overnight. Cells were then treated with FG4592 (100 μM) for 16 hours. RNA was isolated from cultured tissue or using TRIzol chloroform extraction method. RNA was reverse transcribed using MMLV reverse transcriptase (ThermoFisher). qPCR analysis was done using indicated primers (hHILPDA FP: AAGCATGTGTTGAACCTCTACC, RP: TGTGTTGGCTAGTTGGCTTCT; hPLIN2 FP: ATGGCATCCGTTGCAGTTGAT, RP: GGACATGAGGTCATACGTGGAG; mHILPDA FP: TTTCCTTCTGAGGATCTAGC, RP: GACTCCATCACTCTAACAAAG; mPLIN2 FP: GACAGGATGGAGGAAAGACTGC, RP: GGTAGTCGTCACCACATCCTTC) and Radiant Green qPCR master mix (Alkali Scientific Inc.). RNA-seq analysis was performed using data from HIF2α overexpressing colons (GSE173363).

Xenograft Studies

Animal experiments were conducted in accordance with the Office of Laboratory Animal Welfare and approved by the Institutional Animal Care and Use Committees of the University of Michigan. Immunocompromised, 6-8 or 8-10 weeks old of both sexes, were maintained in the facilities of the Unit for Laboratory Animal Medicine (ULAM) under specific pathogen-free conditions. For subcutaneous xenograft studies HCT116, SW480 and DLD1 or sh scrambled and sh HIF-2α HCT116 cells were trypsinzied and 2 million cells were implanted into the lower flanks. All treatments began on day 10 after visible tumor size. DMF (300mg) was mixed in

animal chow (1kg) and this diet was fed to mice. FG4592 was injected intraperitoneally for 7 days continuously at a concentration of 10mg/kg of mouse body weight. Subcutaneous tumor size was measured with digital calipers at the indicated timepoints. Tumor volume (V) was calculated as V = 1/2(length x width2). At endpoint, mice were sacrificed, and tumors were excised. The final tumor volume and weight were measured, and tissue was used for proliferation and apoptosis assay.

Statistical Analysis

Data represent the mean ± SD unless otherwise indicated in figure legends. Data are from three independent experiments measured in triplicate, unless otherwise stated in the figure legend. For statistical analyses, unpaired t-tests were conducted to assess the differences between two groups. One-way or two-way ANOVA was used for multiple treatment conditions followed by Tukey's Post-hoc test. A *P* value of less than 0.05 was considered to be statistically significant. All statistical tests were carried out using Prism 8 software (GraphPad).

Acknowledgements

This work was supported by grants from the National Institutes of Health (R01CA148828, R01CA245546, and R01DK095201) to Y.M.S; (R37CA237421, and R01CA248160) to C.A.L; (R01CA244931, and R01CA215607) to C.A.L. and K.P.O; the UMCCC Core Grant (P30CA046592) to C.A.L. and Y.S; (R35GM130183) to R.B. The University of Michigan GI SPORE Molecular Pathology and Biosample Core (P50CA130810), Center for Gastrointestinal Research (DK034933) and the Department of Defense (CA171086) to Y.M.S. S.A.K. was supported by NIH F31 Predoctoral Fellowship. P.S was supported by NIH/NCI T32 Training Grant in Cancer Biology (5T32CA009676-27). Metabolomics studies performed at the

University of Michigan were supported by NIH grant DK097153, the Charles Woodson Research Fund, and the UM Pediatric Brain Tumor Initiative. Authors thank Dr. Megan Radyk, Rogel Cancer Center and Wesley Huang, Cellular and Molecular Biology, University of Michigan-Medical School for their help in troubleshooting, suggestions, and advice in 4-HNE staining.

Author Contributions

Y.M S. and R.S. conceived the project. R.S., S.R.M., N.K.D., S.A.K., P.S., S.S., A.A., V.V. and R.K. performed experiments and analyzed data. K.P.O., R.B. and C.A.L. provided critical reagents for the study and experimental direction. Y.M.S. and R.S. wrote the manuscript with critical input from all authors.

References

1. Bhandari A, Woodhouse M, and Gupta S. Colorectal cancer is a leading cause of cancer incidence and mortality among adults younger than 50 years in the USA: a SEER-based analysis with comparison to other young-onset cancers. *J Investig Med.* 2017;65(2):311-5.
2. Rawla P, Sunkara T, and Barsouk A. Epidemiology of colorectal cancer: incidence, mortality, survival, and risk factors. *Prz Gastroenterol.* 2019;14(2):89-103.
3. Yu S, Zhou R, Yang T, Liu S, Cui Z, Qiao Q, et al. Hypoxia promotes colorectal cancer cell migration and invasion in a SIRT1-dependent manner. *Cancer Cell Int.* 2019;19:116.
4. Krock BL, Skuli N, and Simon MC. Hypoxia-induced angiogenesis: good and evil. *Genes Cancer.* 2011;2(12):1117-33.
5. Semenza GL. Hypoxia-inducible factors: mediators of cancer progression and targets for cancer therapy. *Trends Pharmacol Sci.* 2012;33(4):207-14.
6. Semenza GL. Hypoxia, clonal selection, and the role of HIF-1 in tumor progression. *Crit Rev Biochem Mol Biol.* 2000;35(2):71-103.
7. Wang GL, Jiang BH, Rue EA, and Semenza GL. Hypoxia-inducible factor 1 is a basic-helix-loop-helix-PAS heterodimer regulated by cellular O2 tension. *Proc Natl Acad Sci U S A.* 1995;92(12):5510-4.
8. Semenza GL. HIF-1: upstream and downstream of cancer metabolism. *Current opinion in genetics & development.* 2010;20(1):51-6.
9. Semenza GL. Hypoxia-inducible factors in physiology and medicine. *Cell.* 2012;148(3):399-408.
10. Imamura T, Kikuchi H, Herraiz MT, Park DY, Mizukami Y, Mino-Kenduson M, et al. HIF-1alpha and HIF-2alpha have divergent roles in colon cancer. *Int J Cancer.* 2009;124(4):763-71.
11. Keith B, Johnson RS, and Simon MC. HIF1alpha and HIF2alpha: sibling rivalry in hypoxic tumour growth and progression. *Nature reviews Cancer.* 2011;12(1):9-22.
12. Ramakrishnan SK, and Shah YM. Role of Intestinal HIF-2alpha in Health and Disease. *Annu Rev Physiol.* 2016;78:301-25.
13. Yoshimura H, Dhar DK, Kohno H, Kubota H, Fujii T, Ueda S, et al. Prognostic impact of hypoxia-inducible factors 1alpha and 2alpha in colorectal cancer patients: correlation with tumor angiogenesis and cyclooxygenase-2 expression. *Clin Cancer Res.* 2004;10(24):8554-60.
14. Xue X, Ramakrishnan SK, and Shah YM. Activation of HIF-1alpha does not increase intestinal tumorigenesis. *Am J Physiol Gastrointest Liver Physiol.* 2014;307(2):G187-95.
15. Ma X, Zhang H, Xue X, and Shah YM. Hypoxia-inducible factor 2alpha (HIF-2alpha) promotes colon cancer growth by potentiating Yes-associated protein 1 (YAP1) activity. *J Biol Chem.* 2017;292(41):17046-56.
16. Xue X, Ramakrishnan SK, Weisz K, Triner D, Xie L, Attili D, et al. Iron Uptake via DMT1 Integrates Cell Cycle with JAK-STAT3 Signaling to Promote Colorectal Tumorigenesis. *Cell metabolism.* 2016;24(3):447-61.

17. Xue X, Taylor M, Anderson E, Hao C, Qu A, Greenson JK, et al. Hypoxia-inducible factor-2alpha activation promotes colorectal cancer progression by dysregulating iron homeostasis. *Cancer Res.* 2012;72(9):2285-93.
18. Shay JE, Imtiyaz HZ, Sivanand S, Durham AC, Skuli N, Hsu S, et al. Inhibition of hypoxia-inducible factors limits tumor progression in a mouse model of colorectal cancer. *Carcinogenesis.* 2014;35(5):1067-77.
19. Triner D, and Shah YM. Hypoxia-inducible factors: a central link between inflammation and cancer. *J Clin Invest.* 2016;126(10):3689-98.
20. Scheuermann TH, Tomchick DR, Machius M, Guo Y, Bruick RK, and Gardner KH. Artificial ligand binding within the HIF2alpha PAS-B domain of the HIF2 transcription factor. *Proc Natl Acad Sci U S A.* 2009;106(2):450-5.
21. Chen W, Hill H, Christie A, Kim MS, Holloman E, Pavia-Jimenez A, et al. Targeting renal cell carcinoma with a HIF-2 antagonist. *Nature.* 2016;539(7627):112-7.
22. Cho H, Du X, Rizzi JP, Liberzon E, Chakraborty AA, Gao W, et al. On-target efficacy of a HIF-2alpha antagonist in preclinical kidney cancer models. *Nature.* 2016;539(7627):107-11.
23. Dixon SJ, Lemberg KM, Lamprecht MR, Skouta R, Zaitsev EM, Gleason CE, et al. Ferroptosis: an iron-dependent form of nonapoptotic cell death. *Cell.* 2012;149(5):1060-72.
24. Stockwell BR, Friedmann Angeli JP, Bayir H, Bush AI, Conrad M, Dixon SJ, et al. Ferroptosis: A Regulated Cell Death Nexus Linking Metabolism, Redox Biology, and Disease. *Cell.* 2017;171(2):273-85.
25. Lang X, Green MD, Wang W, Yu J, Choi JE, Jiang L, et al. Radiotherapy and Immunotherapy Promote Tumoral Lipid Oxidation and Ferroptosis via Synergistic Repression of SLC7A11. *Cancer Discov.* 2019;9(12):1673-85.
26. Wang W, Green M, Choi JE, Gijon M, Kennedy PD, Johnson JK, et al. CD8(+) T cells regulate tumour ferroptosis during cancer immunotherapy. *Nature.* 2019;569(7755):270-4.
27. Badgley MA, Kremer DM, Maurer HC, DelGiorno KE, Lee HJ, Purohit V, et al. Cysteine depletion induces pancreatic tumor ferroptosis in mice. *Science.* 2020;368(6486):85-9.
28. Xu Z, Zhang F, Sun F, Gu K, Dong S, and He D. Dimethyl fumarate for multiple sclerosis. *Cochrane Database Syst Rev.* 2015(4):CD011076.
29. Stangel M, and Linker RA. Dimethyl fumarate (BG-12) for the treatment of multiple sclerosis. *Expert Rev Clin Pharmacol.* 2013;6(4):355-62.
30. Ashrafian H, Czibik G, Bellahcene M, Aksentijevic D, Smith AC, Mitchell SJ, et al. Fumarate is cardioprotective via activation of the Nrf2 antioxidant pathway. *Cell Metab.* 2012;15(3):361-71.
31. Pitarokoili K, Ambrosius B, Meyer D, Schrewe L, and Gold R. Dimethyl Fumarate Ameliorates Lewis Rat Experimental Autoimmune Neuritis and Mediates Axonal Protection. *PLoS One.* 2015;10(11):e0143416.
32. Papadopoulou A, D'Souza M, Kappos L, and Yaldizli O. Dimethyl fumarate for multiple sclerosis. *Expert Opin Investig Drugs.* 2010;19(12):1603-12.
33. Scannevin RH, Chollate S, Jung MY, Shackett M, Patel H, Bista P, et al. Fumarates promote cytoprotection of central nervous system cells against oxidative stress via the

nuclear factor (erythroid-derived 2)-like 2 pathway. *J Pharmacol Exp Ther.* 2012;341(1):274-84.
34. Xie X, Zhao Y, Ma CY, Xu XM, Zhang YQ, Wang CG, et al. Dimethyl fumarate induces necroptosis in colon cancer cells through GSH depletion/ROS increase/MAPKs activation pathway. *Br J Pharmacol.* 2015;172(15):3929-43.
35. Loewe R, Valero T, Kremling S, Pratscher B, Kunstfeld R, Pehamberger H, et al. Dimethylfumarate impairs melanoma growth and metastasis. *Cancer Res.* 2006;66(24):11888-96.
36. Yamazoe Y, Tsubaki M, Matsuoka H, Satou T, Itoh T, Kusunoki T, et al. Dimethylfumarate inhibits tumor cell invasion and metastasis by suppressing the expression and activities of matrix metalloproteinases in melanoma cells. *Cell Biol Int.* 2009;33(10):1087-94.
37. Yang M, Soga T, Pollard PJ, and Adam J. The emerging role of fumarate as an oncometabolite. *Front Oncol.* 2012;2:85.
38. Feng Y, Bommer GT, Zhao J, Green M, Sands E, Zhai Y, et al. Mutant KRAS promotes hyperplasia and alters differentiation in the colon epithelium but does not expand the presumptive stem cell pool. *Gastroenterology.* 2011;141(3):1003-13 e1-10.
39. Solanki S, Devenport SN, Ramakrishnan SK, and Shah YM. Temporal induction of intestinal epithelial hypoxia-inducible factor-2alpha is sufficient to drive colitis. *Am J Physiol Gastrointest Liver Physiol.* 2019;317(2):G98-G107.
40. Zou Y, Palte MJ, Deik AA, Li H, Eaton JK, Wang W, et al. A GPX4-dependent cancer cell state underlies the clear-cell morphology and confers sensitivity to ferroptosis. *Nat Commun.* 2019;10(1):1617.
41. Kappos L, Gold R, Miller DH, Macmanus DG, Havrdova E, Limmroth V, et al. Efficacy and safety of oral fumarate in patients with relapsing-remitting multiple sclerosis: a multicentre, randomised, double-blind, placebo-controlled phase IIb study. *Lancet.* 2008;372(9648):1463-72.
42. Sullivan LB, Martinez-Garcia E, Nguyen H, Mullen AR, Dufour E, Sudarshan S, et al. The proto-oncometabolite fumarate binds glutathione to amplify ROS-dependent signaling. *Mol Cell.* 2013;51(2):236-48.
43. Perez M, Bak DW, Bergholtz SE, Crooks DR, Arimilli BS, Yang Y, et al. Heterogeneous adaptation of cysteine reactivity to a covalent oncometabolite. *J Biol Chem.* 2020.
44. Kornberg MD, Bhargava P, Kim PM, Putluri V, Snowman AM, Putluri N, et al. Dimethyl fumarate targets GAPDH and aerobic glycolysis to modulate immunity. *Science.* 2018;360(6387):449-53.
45. Lee HJ, Kremer DM, Sajjakulnukit P, Zhang L, and Lyssiotis CA. A large-scale analysis of targeted metabolomics data from heterogeneous biological samples provides insights into metabolite dynamics. *Metabolomics.* 2019;15(7):103.
46. Halbrook CJ, Pontious C, Kovalenko I, Lapienyte L, Dreyer S, Lee HJ, et al. Macrophage-Released Pyrimidines Inhibit Gemcitabine Therapy in Pancreatic Cancer. *Cell Metab.* 2019;29(6):1390-9 e6.
47. Swain A, Bambouskova M, Kim H, Andhey PS, Duncan D, Auclair K, et al. Comparative evaluation of itaconate and its derivatives reveals divergent inflammasome and type I interferon regulation in macrophages. *Nat Metab.* 2020;2(7):594-602.
48. Semenza GL. Hypoxia-inducible factor 1: regulator of mitochondrial metabolism and mediator of ischemic preconditioning. *Biochim Biophys Acta.* 2011;1813(7):1263-8.

49. Triner D, Xue X, Schwartz AJ, Jung I, Colacino JA, and Shah YM. Epithelial Hypoxia-Inducible Factor 2alpha Facilitates the Progression of Colon Tumors through Recruiting Neutrophils. *Mol Cell Biol.* 2017;37(5).
50. Shah YM, Matsubara T, Ito S, Yim SH, and Gonzalez FJ. Intestinal hypoxia-inducible transcription factors are essential for iron absorption following iron deficiency. *Cell Metab.* 2009;9(2):152-64.
51. Cadet J, and Davies KJA. Oxidative DNA damage & repair: An introduction. *Free Radic Biol Med.* 2017;107:2-12.
52. Siddiqui MS, Francois M, Fenech MF, and Leifert WR. Persistent gammaH2AX: A promising molecular marker of DNA damage and aging. *Mutat Res Rev Mutat Res.* 2015;766:1-19.
53. Filipovic MR, Zivanovic J, Alvarez B, and Banerjee R. Chemical Biology of H2S Signaling through Persulfidation. *Chem Rev.* 2018;118(3):1253-337.
54. Yadav PK, Vitvitsky V, Carballal S, Seravalli J, and Banerjee R. Thioredoxin regulates human mercaptopyruvate sulfurtransferase at physiologically-relevant concentrations. *J Biol Chem.* 2020;295(19):6299-311.
55. Wang GL, and Semenza GL. Molecular basis of hypoxia-induced erythropoietin expression. *Curr Opin Hematol.* 1996;3(2):156-62.
56. Wang GL, and Semenza GL. General involvement of hypoxia-inducible factor 1 in transcriptional response to hypoxia. *Proc Natl Acad Sci U S A.* 1993;90(9):4304-8.
57. van der Reest J, Lilla S, Zheng L, Zanivan S, and Gottlieb E. Proteome-wide analysis of cysteine oxidation reveals metabolic sensitivity to redox stress. *Nat Commun.* 2018;9(1):1581.
58. Zivanovic J, Kouroussis E, Kohl JB, Adhikari B, Bursac B, Schott-Roux S, et al. Selective Persulfide Detection Reveals Evolutionarily Conserved Antiaging Effects of S-Sulfhydration. *Cell Metab.* 2019;30(6):1152-70 e13.
59. Wedmann R, Onderka C, Wei S, Szijarto IA, Miljkovic JL, Mitrovic A, et al. Improved tag-switch method reveals that thioredoxin acts as depersulfidase and controls the intracellular levels of protein persulfidation. *Chem Sci.* 2016;7(5):3414-26.
60. Izquierdo-Alvarez A, Ramos E, Villanueva J, Hernansanz-Agustin P, Fernandez-Rodriguez R, Tello D, et al. Differential redox proteomics allows identification of proteins reversibly oxidized at cysteine residues in endothelial cells in response to acute hypoxia. *J Proteomics.* 2012;75(17):5449-62.
61. Libiad M, Vitvitsky V, Bostelaar T, Bak DW, Lee HJ, Sakamoto N, et al. Hydrogen sulfide perturbs mitochondrial bioenergetics and triggers metabolic reprogramming in colon cells. *J Biol Chem.* 2019;294(32):12077-90.
62. Taniguchi CM, Miao YR, Diep AN, Wu C, Rankin EB, Atwood TF, et al. PHD inhibition mitigates and protects against radiation-induced gastrointestinal toxicity via HIF2. *Sci Transl Med.* 2014;6(236):236ra64.
63. Samanta D, and Semenza GL. Maintenance of redox homeostasis by hypoxia-inducible factors. *Redox Biol.* 2017;13:331-5.
64. Zhang Y, Tan H, Daniels JD, Zandkarimi F, Liu H, Brown LM, et al. Imidazole Ketone Erastin Induces Ferroptosis and Slows Tumor Growth in a Mouse Lymphoma Model. *Cell Chem Biol.* 2019;26(5):623-33 e9.

65. Yuan M, Kremer DM, Huang H, Breitkopf SB, Ben-Sahra I, Manning BD, et al. Ex vivo and in vivo stable isotope labelling of central carbon metabolism and related pathways with analysis by LC-MS/MS. *Nat Protoc.* 2019;14(2):313-30.
66. Dame MK, Jiang Y, Appelman HD, Copley KD, McClintock SD, Aslam MN, et al. Human colonic crypts in culture: segregation of immunochemical markers in normal versus adenoma-derived. *Laboratory investigation; a journal of technical methods and pathology.* 2014;94(2):222-34.

Figure 1

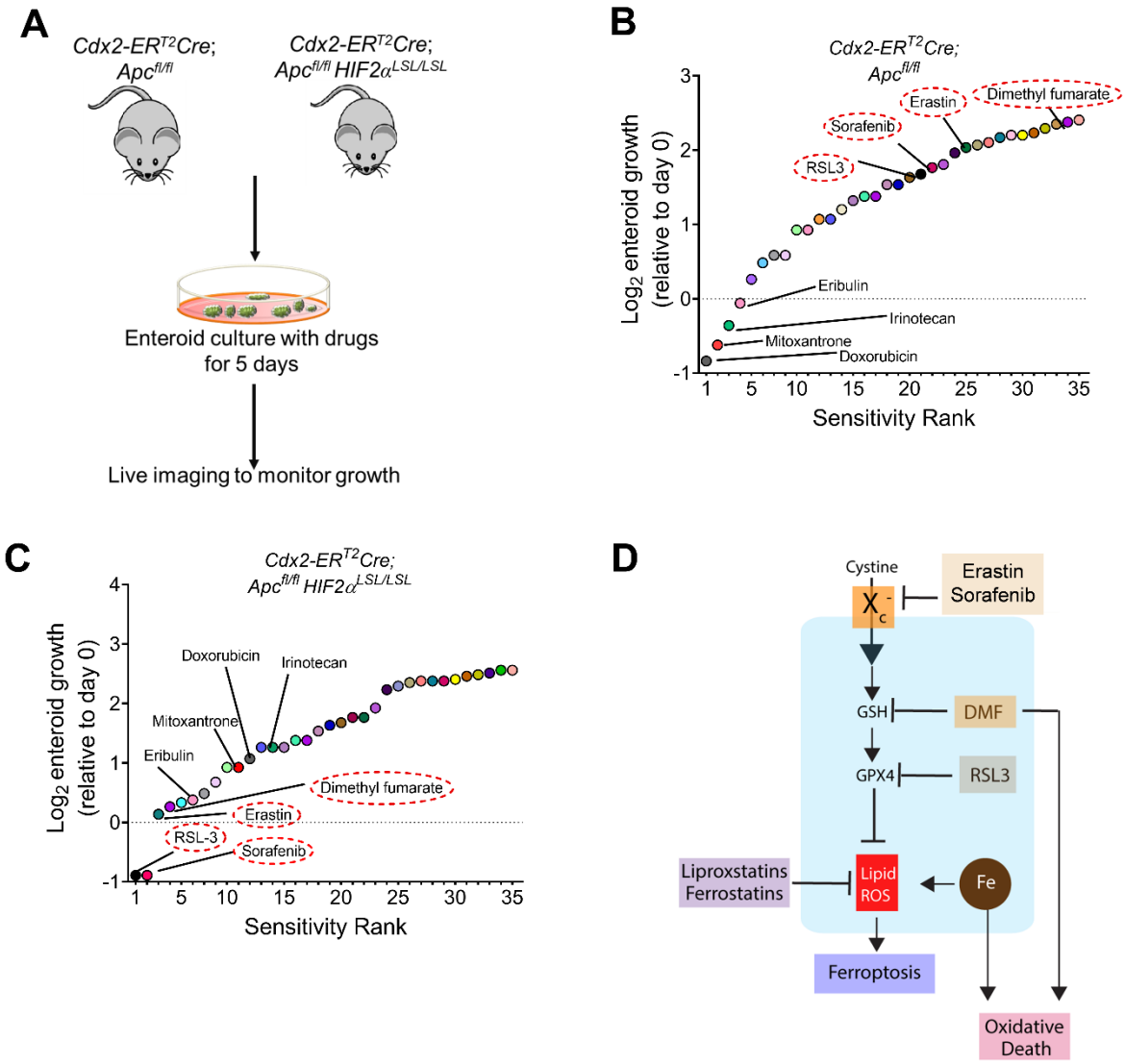

Figure 1. Screening of compounds that exhibit reduction in growth of HIF-2α overexpressing tumor enteroids. (A) Schematic of enteroids isolated from a sporadic colon cancer mouse model (Cdx2-ER^{T2}Cre; *Apc$^{fl/fl}$*) and colon cancer HIF-2α overexpressing mouse model (Cdx2-ER^{T2}Cre; *Apc$^{fl/fl}$HIF2α$^{LSL/LSL}$*). **(B & C)** Log$_2$ fold change in area under the curve (AUC) from cell viability dose response curves for each compound in the library, signifying the most sensitive (1) to least sensitive (35) compounds (n=10). **(D)** Schematic of known oxidative cell death pathways of the four most significant compounds from the screen, indicating ferroptosis activators such as erastin, RSL3 and sorafenib that inhibit *Slc7a11* or GPX4 and induce lipid peroxides. The process of lipid reactive oxygen species (Li-ROS) accumulation can be inhibited by ferroptosis inhibitors such as ferrostatins and liproxstatins which directly eliminate lipid peroxide formation. Small molecules like DMF are known to mediate oxidative stress and cell death by depletion of GSH.

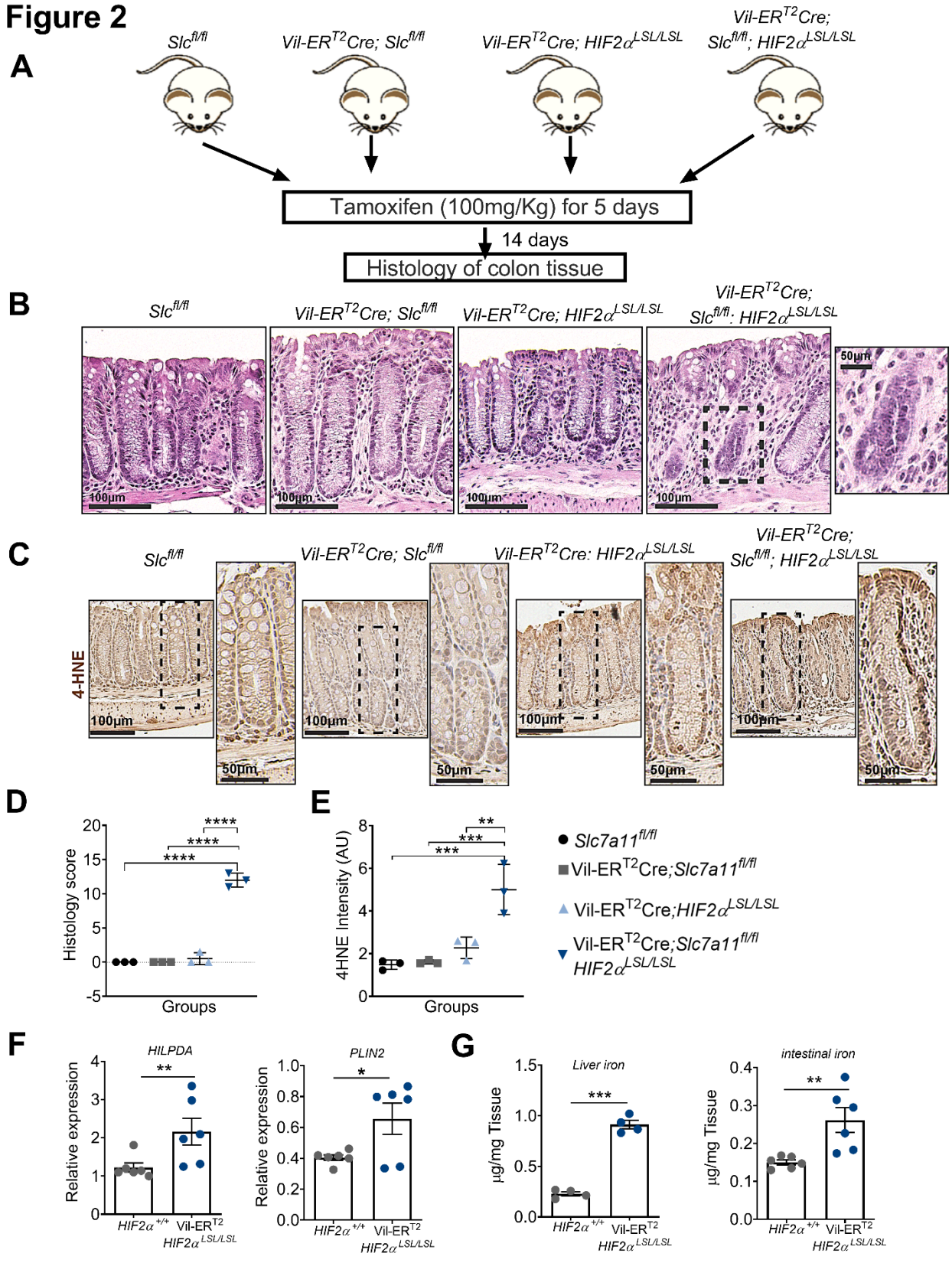

Figure 2. HIF-2α activation potentiates ferroptosis *in vivo*. (A) Schematic of temporal

activation of intestinal HIF-2α and deletion of *Slc7a11* in the colon following tamoxifen treatment (100mg/Kg). **(B)** Representative hematoxylin-and-eosin staining or **(C)** immunohistochemistry analysis showing 4-HNE of colons from a *Slc7a11*$^{fl/fl}$, Vil-ER^{T2}Cre; *Slc7a11*$^{fl/fl}$, Vil-ER^{T2}Cre; *HIF2α*$^{LSL/LSL}$ and Vil-ER^{T2}Cre; *Slc7a11*$^{fl/fl}$; *HIF2α*$^{LSL/LSL}$ mice. Quantitation of histology score **(D)** and (E) 4-HNE (n=3 in each group). One-way ANOVA followed by Tukey's multiple comparisons test was used for comparison between groups, **P<0.01, ***p<0.001 and ****P<0.0001. **(F)** qRT-PCR analysis for HILPDA and PLIN2 in *HIF-2α*$^{+/+}$ (n=6) and Vil-ER^{T2}*HIF2α*$^{LSL/LSL}$ mice (n=6). **(G)** Iron levels measured in liver (n=4) and intestinal tissue (n=6) in *HIF-2α*$^{+/+}$ and Vil-ER^{T2}*HIF2α*$^{LSL/LSL}$ mice. Data represent mean ± SD from 3 independent experiments. *P* values were determined using unpaired t-test; *P<0.05, **P<0.01, ***P<0.001, for the differences between different groups as indicated in figure.

Figure 3

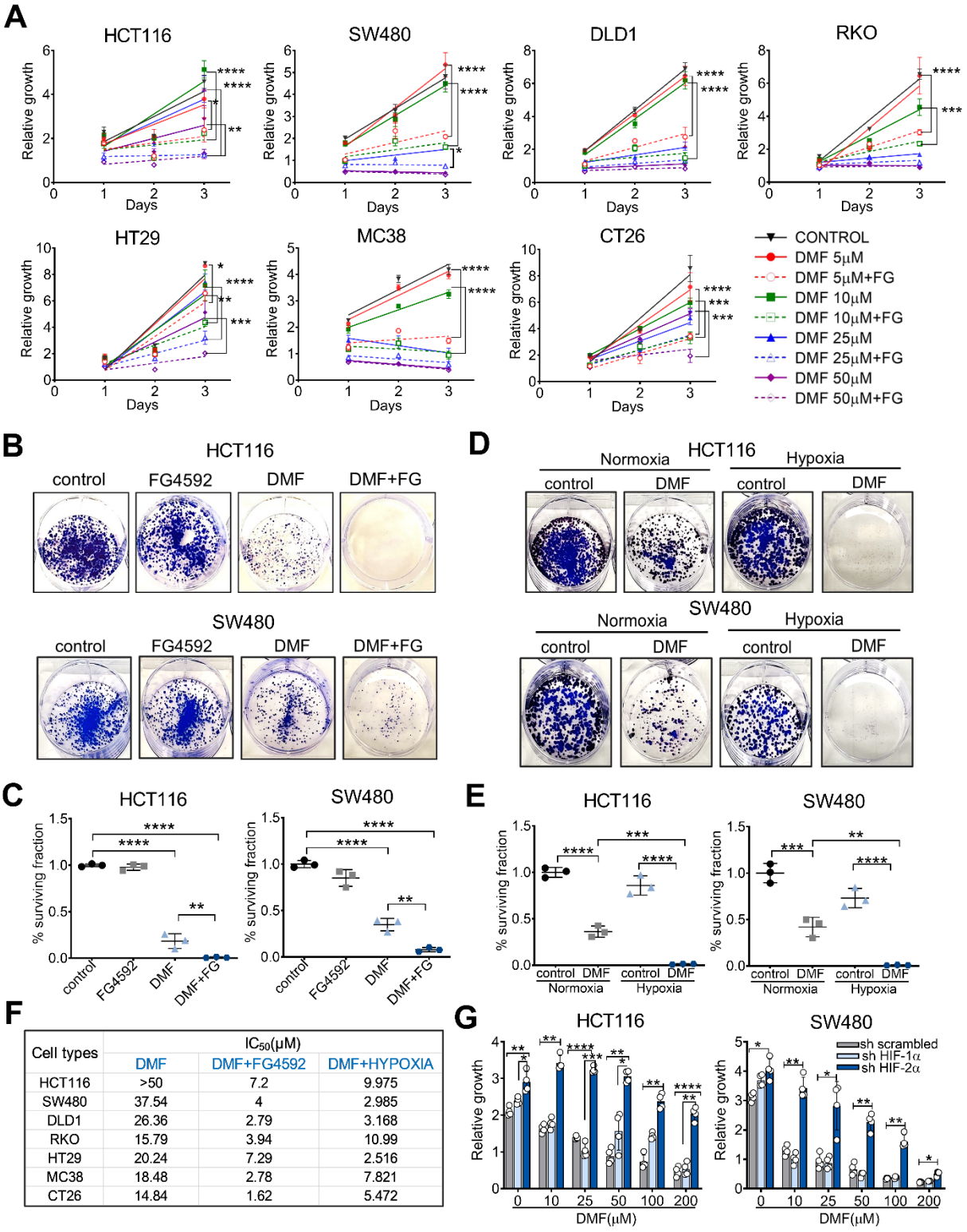
A
HCT116
SW480
DLD1
RKO
HT29
MC38
CT26
Relative growth
Days
CONTROL
DMF 5μM
DMF 5μM+FG
DMF 10μM
DMF 10μM+FG
DMF 25μM
DMF 25μM+FG
DMF 50μM
DMF 50μM+FG
B
HCT116
control
FG4592
DMF
DMF+FG
SW480
D
Normoxia
Hypoxia
C
% surviving fraction
E
F
Cell types
IC50(μM)
DMF
DMF+FG4592
DMF+HYPOXIA
HCT116 >50 7.2 9.975
SW480 37.54 4 2.985
DLD1 26.36 2.79 3.168
RKO 15.79 3.94 10.99
HT29 20.24 7.29 2.516
MC38 18.48 2.78 7.821
CT26 14.84 1.62 5.472
G
sh scrambled
sh HIF-1α
sh HIF-2α
DMF(μM)

Figure 3. Hypoxia mimetic contributes to DMF induced growth inhibition in CRC cells. (A) Cell growth assay following FG4592 (100μM) and DMF co-treatment. Error bars represent mean ± SD. Statistical significance was calculated using one-way ANOVA followed by Tukey's multiple comparisons test. *P<0.05, ** P<0.01, ***P< 0.001, ****P<0.0001. **(B)** Representative images and **(C)** quantitation of colony forming assays in HCT116 and SW480 cells treated with DMF (25μM), FG4592 (100μM) or co-treated with DMF and FG4592. **(D)** Representative images and **(E)** quantitation of colony forming assays in HCT116 and SW480 cells treated with DMF (25μM) and cultured under normoxic and hypoxic conditions. Quantitative data represent means ± SD from 3 independent experiments. Statistical significance was calculated using one-way ANOVA with Tukey's multiple comparisons. **P<0.01, ***P<0.001, ****p<0.0001 **(F)** Table showing IC_{50} values in a panel of CRC cells treated with DMF (5-50μM) either alone and in combination with FG4592 (100μM) or hypoxia **(G)** Growth assay of HIF-1α and HIF-2α knockdown in HCT116 and SW480 cells treated with DMF alone or in combination with FG4592 (100μM). Quantitative data represent means ± SD from 3 independent experiments. Statistical significance was calculated using two-way ANOVA with Tukey's multiple comparisons. *P<0.05, **P<0.01, ***P<0.001, ****p<0.0001

Figure 4

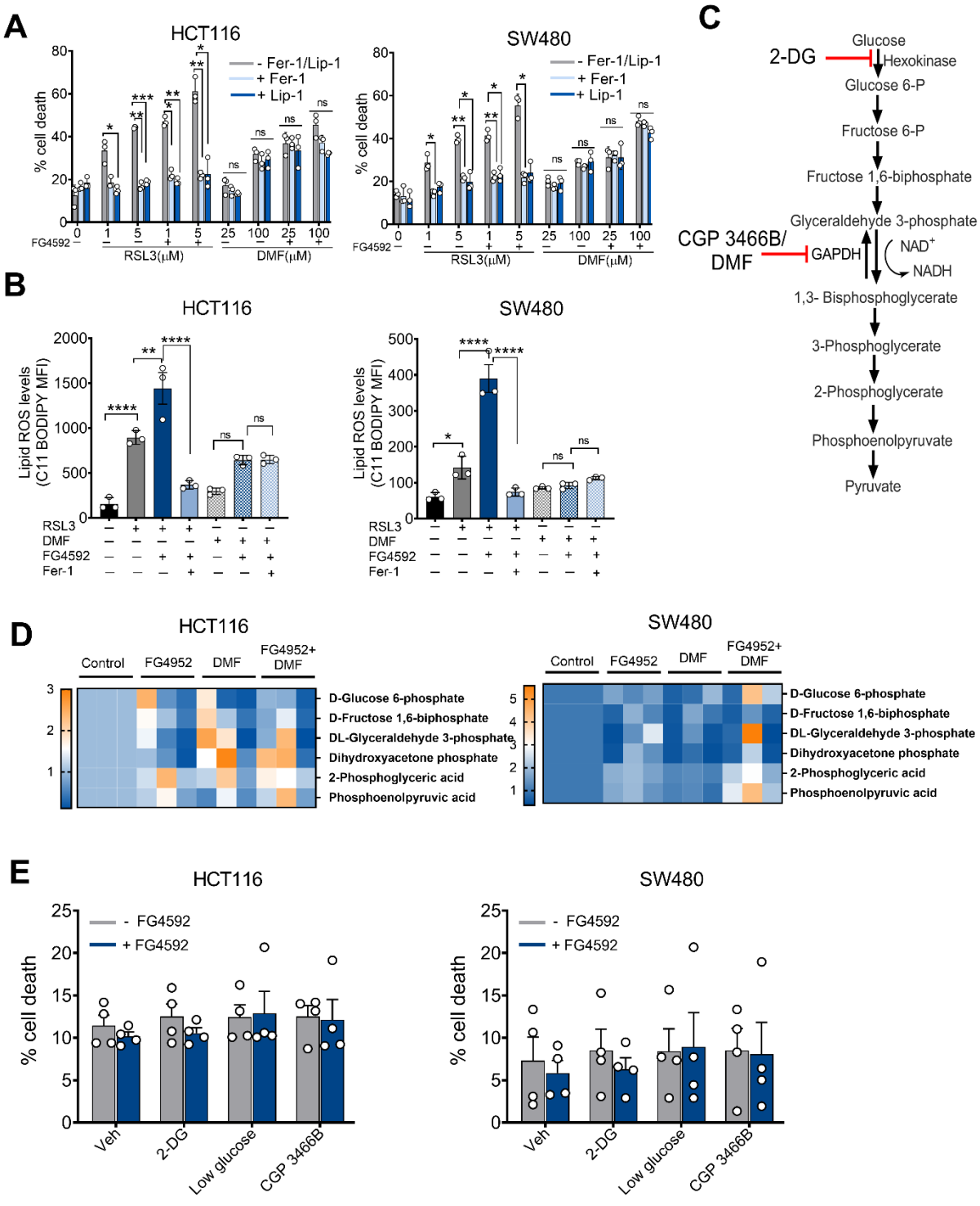

Figure 4. DMF is not a ferroptotic inducer in CRC cells. (A) HCT116 and SW480 cells were treated with RSL3 (1 and 5μM) or DMF (25 and 100μM) alone or in combination with FG4592(100μM) with or without ferroptotic inhibitors; ferrostatin-1 (0.5μM) or liproxstatin-1

(1μM) for 24 h and cell death was assayed. Data are means ± SD from three independent experiments. Statistical significance was calculated using two-way ANOVA with Tukey's multiple comparison test. *P<0.05, **P<0.01, ***P<0.001, ns=non-significant. **(B)** HCT116 and SW480 cells were treated with RSL3 (2μM), DMF (50μM) or in combination with FG4592(100μM) with or without ferrostatin-1 (1μM) for 12 hours. Lipid ROS was determined in these cells through staining with ferroptosis-dependent C11-BODIPY581/591. Data are plotted as the mean ± SD. *P* values were determined using one-way ANOVA with Tukey's multiple comparison; **P* <0.05, ***P* < 0.01, ****P<0.0001, ns=nonsignificant. **(C)** Schematic of glycolysis pathway in cells showing DMF, CGP 3466B as inhibitors of GAPDH and 2-DG as inhibitor of hexokinase. (**D**) Heatmap showing the relative abundance of glycolytic intermediates in HCT116 and SW480 cells treated with FG4592 (100μM) or DMF (50μM) either alone or in combination. **(E)** HCT116 and SW480 cells were treated with glycolysis inhibitors with or without FG4592 and cell death was assessed using LDH assay.

Figure 5

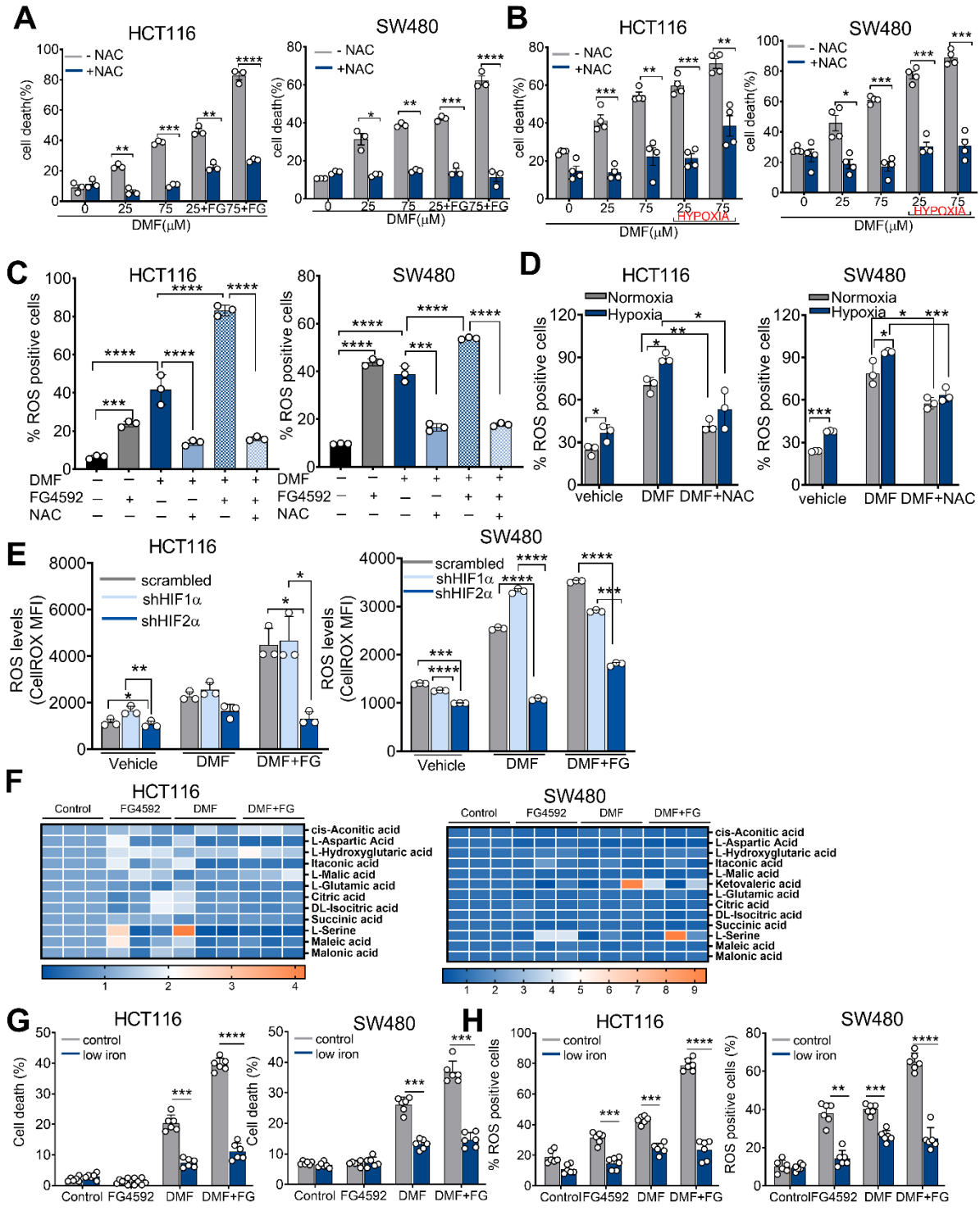

Figure 5. ROS generation and iron accumulation are involved in DMF and FG4592-mediated cell death in CRC cells. Cell death assay in HCT116 and SW480 cells treated with DMF (25 and 75μM) **(A)** co-treated with DMF and FG4592 (100μM) **(B)** cultured under hypoxia

with or without N-acetyl cysteine (NAC) (5mM). Data represent means ± SD from three independent experiments. Statistical significance was calculated using unpaired-t test. *p<0.05, **P<0.01, ***P <0.001, ****P < 0.0001. ROS measurements in HCT116 and SW480 cells (**C**) treated with FG4592 (100μM), DMF (50μM) or DMF and FG4592 with or without NAC. **(D)** treated with DMF and cultured in normoxia and hypoxia with or without NAC. Data are plotted as the mean ± SD from 3 independent experiments. Statistical significance was calculated using one-way ANOVA with Tukey's multiple comparison test. *P<0.05, **P <0.01, ***P < 0.001, ****P < 0.0001. **(E)** ROS measurement in shRNA mediated HIF-1α, HIF-2α knock-down and non-target scrambled HCT116 and SW480 cells treated with DMF (50μM) either alone or in combination with FG4592 (100μM). Statistical significance was calculated using two-way ANOVA with Tukey's multiple comparison, ***P<0.001, ****P <0.0001, **(F)** Heatmap showing the relative abundance of mitochondrial metabolites in FG4592 (100μM) and DMF (50μM) treated HCT116 and SW480 cells. **(G)** Cell death and **(H)** ROS measurement in FG4592 (100μM), DMF (75 μM) either alone or co-treated conditions in the presence of normal iron (control) and low iron. Statistical significance was calculated using unpaired t-test, **P <0.01, ***P < 0.001, ****P < 0.0001.

Figure 6

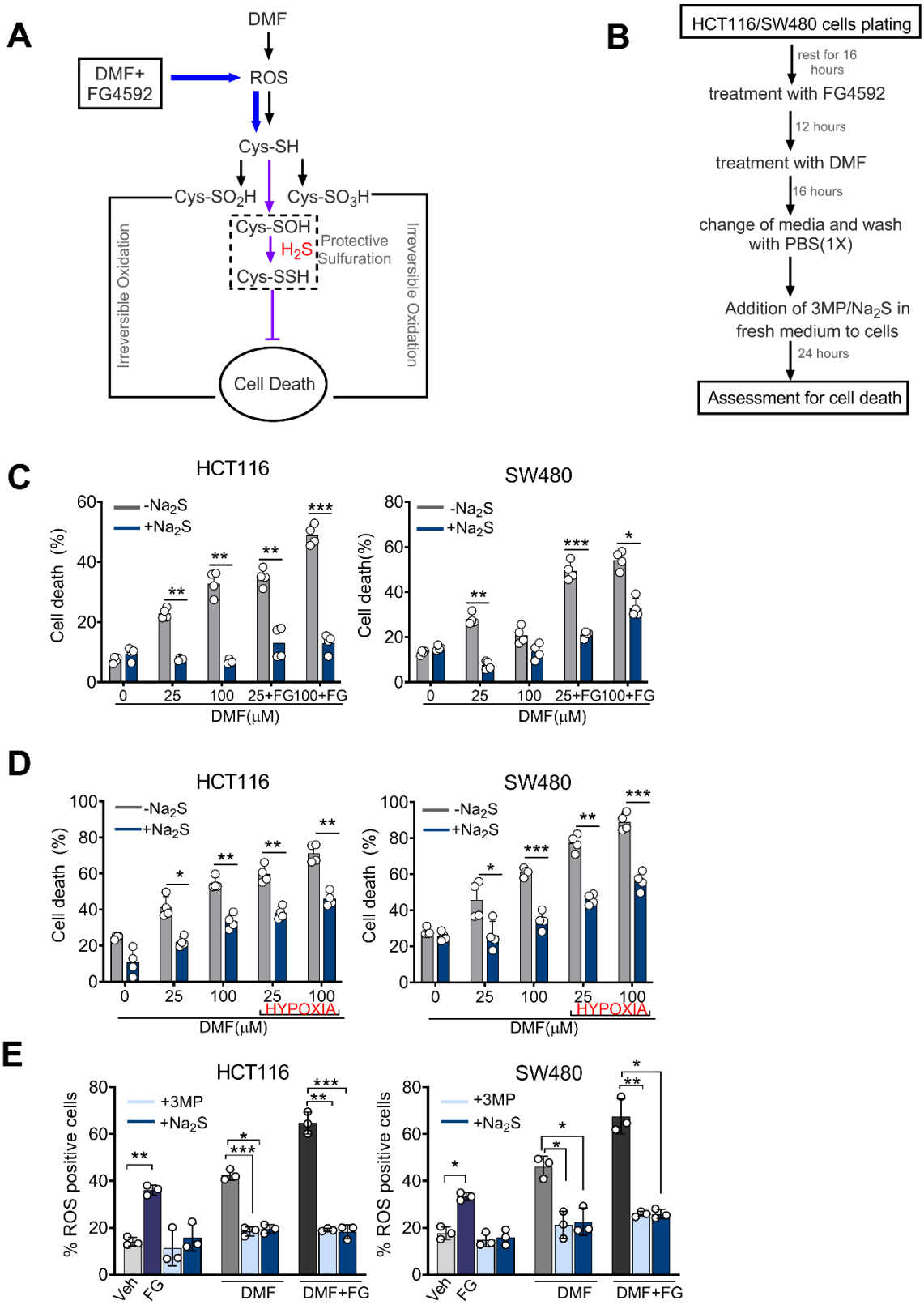

Figure 6. H_2S can prevent irreversible protein oxidation and rescue cell death mediated by

DMF and FG4592. (A) Schematic showing H_2S effects on DMF-mediated cell death. The addition of sulphur group to proteins prevents the cell death mediated by DMF. **(B)** Schematic showing treatment regime of HCT116 and SW480 cells with DMF, FG4592, 3MP and Na_2S **(C & D)** Cell death in HCT116 and SW480 cells treated with DMF (25 and 100μM) **(C)** co-treated with DMF and FG4592 (100μM) **(D)** cultured under normoxic and hypoxic conditions with or without Na_2S (300μM). Data represent means ± SD from three independent experiments. Statistical significance was calculated using unpaired-t test. *p<0.05, **P<0.01, ***P <0.001 **(E)** ROS measurements in HCT116 and SW480 cells treated with DMF (50μM), DMF in combination with FG4592 (100μM) either alone or in addition with 3MP (5mM) and Na_2S (300μM) for 16 hours. Data represent mean ± SD from 3 independent experiments. Statistical significance was calculated using two-way ANOVA with Tukey's multiple comparison, **P <0.01, ***P < 0.001.

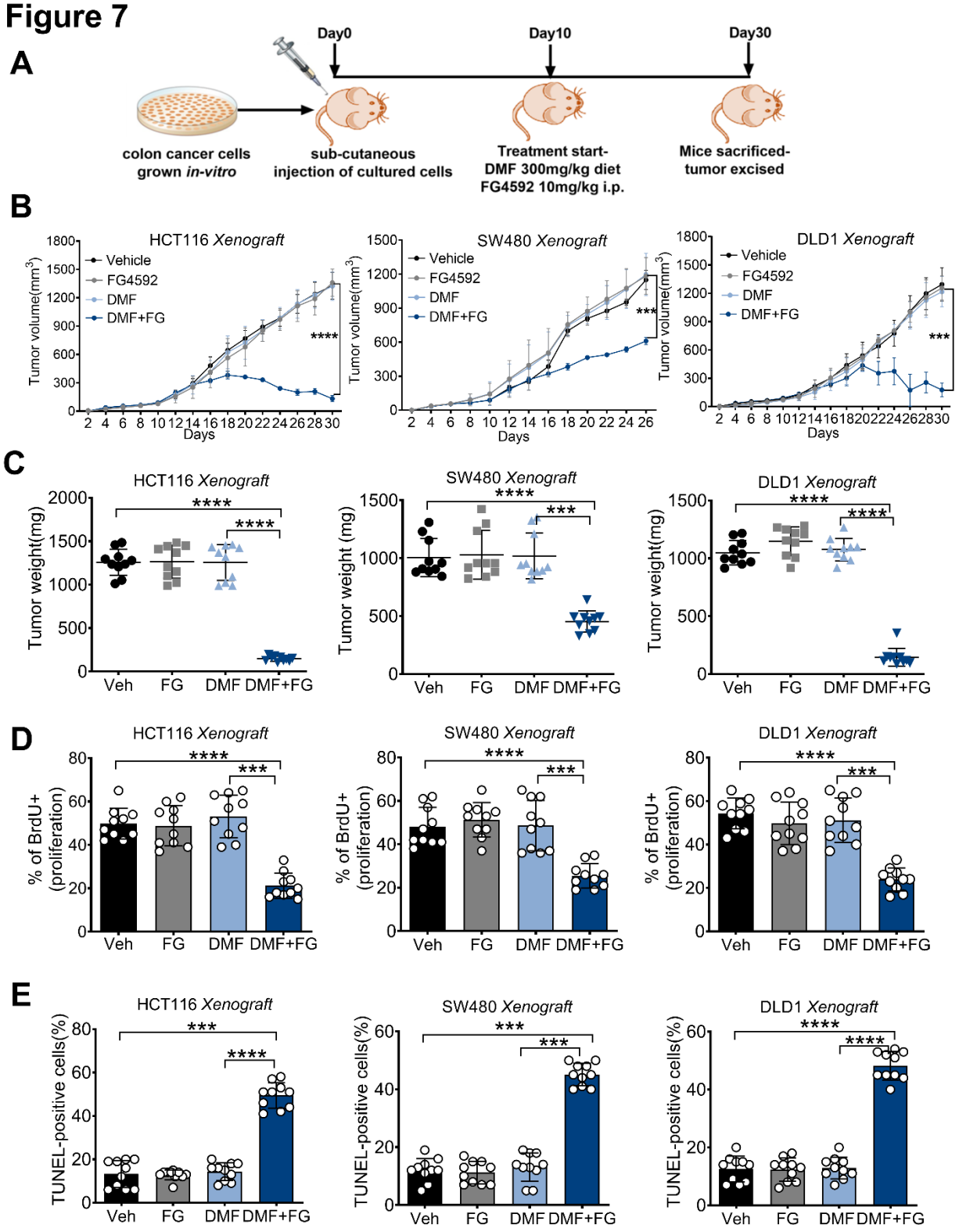

Figure 7. DMF and FG4592 potentiate CRC cell death *in vivo*. (**A**) Schematic of xenografts *in vivo* study. HCT116, SW480 and DLD1 cells were injected subcutaneously into both flanks of

C57BL/6 mice (n=10 for each group). After visible formation of tumor at day 10, the mice were subjected to DMF diet (300mg/kg of chow) and FG4592 (10mg/kg of mouse weight). **(B)** Tumor volume **(C)** tumor weight **(D)** tumor proliferation and **(E)** tumor apoptosis in HCT116, SW480 and DLD1 xenograft mice. Data represent mean ± SD. *P<0.05, **P<0.01, ***P < 0.001, ****P < 0.0001(differences between untreated mice and between treated groups), one-way ANOVA with Tukey's multiple comparison test was used for calculating statistical significance.

Figure 8

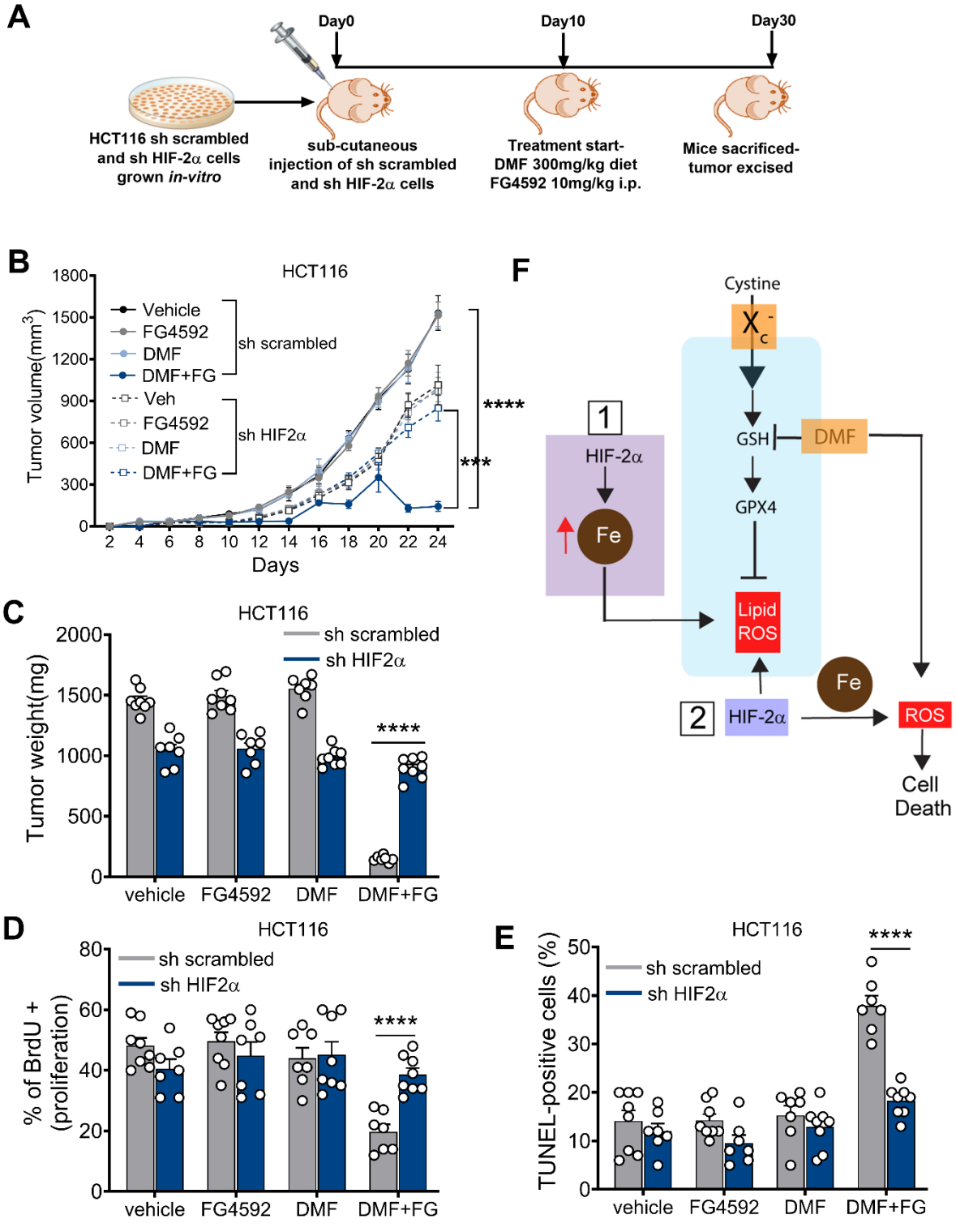

Figure 8. DMF mediated CRC cell death *in vivo* is HIF-2α dependent. (A) Schematic of HIF-2α knock-down xenograft *in vivo* study. shRNA mediated HIF-2α knock-down and non-target scrambled HCT116 cells were injected subcutaneously into both flanks of C57BL/6 mice (n=8

for each group). After visible formation of tumor at day 10, the mice were subjected to DMF diet (300mg/kg of chow) and FG4592 (10mg/kg of mouse body weight). **(B)** Tumor volume **(C)** tumor weight **(D)** tumor proliferation and **(E)** tumor apoptosis in HIF-2α knock-down and non-target scrambled HCT116 xenograft mice. Data represent mean ± SD. ***P < 0.001, ****P < 0.0001(differences between scrambled and HIF-2α knock-down cells for DMF+FG treatment), unpaired t-test was used for calculating statistical significance. **(E)** Schematic outlining the role of HIF-2α mediating vulnerability to oxidative cell death. HIF-2α mediate iron toxicity and accumulation of lipid ROS which synergize with ferroptotic activators to enhance CRC cell death. HIF-2α also increase cellular iron and synergize with cellular oxidants such as DMF to enhance irreversible cysteine oxidation and cell death.